

Optical Constants of $(\text{Al}_{0.98}\text{Ga}_{0.02})_x\text{O}_y$ Native Oxides

K.J. Knopp, R.P. Mirin, D.H. Christensen, K.A. Bertness, and A. Roshko
National Institute of Standards and Technology, Boulder, Colorado

R.A. Synowicki
J.A. Woollam Company Inc., Lincoln, Nebraska

Abstract:

We report the optical constants of oxidized crystalline and low-temperature-grown (LTG) $\text{Al}_{0.98}\text{Ga}_{0.02}\text{As}$ films, as determined by variable angle spectroscopic ellipsometry. Data were acquired at three angles of incidence over 240-1700nm and fit to a Cauchy dispersion function. For oxidized crystalline material, we observe a variation in the real index of $\pm 0.5\%$ for layer thickness variations of $\pm 6\%$. We show that upon oxidation, LTG material can expand by $>25\%$ while crystalline material contracts by $<2\%$. Atomic force microscopy analysis indicates thickness-dependent variations in the oxide microstructure. Additionally, an optical scattering loss of 1.1×10^{-6} is calculated based on surface roughness measurements for a thin layer of oxidized crystalline material.

Optical constants of $(\text{Al}_{0.98}\text{Ga}_{0.02})_x\text{O}_y$ native oxides

K. J. Knopp, R. P. Mirin, D. H. Christensen, K. A. Bertness, and A. Roshko
National Institute of Standards and Technology, 325 Broadway MS 815.04, Boulder, Colorado 80303

R. A. Synowicki
J. A. Woollam Company, Inc., Lincoln, Nebraska 68508

(Received 20 August 1998; accepted 9 October 1998)

We report the optical constants of oxidized crystalline and low-temperature-grown (LTG) $\text{Al}_{0.98}\text{Ga}_{0.02}\text{As}$ films, as determined by variable angle spectroscopic ellipsometry. Data were acquired at three angles of incidence over 240–1700 nm and fitted to a Cauchy dispersion function. For oxidized crystalline material, we observe a variation in the real index of $\pm 0.5\%$ for layer thickness variations of $\pm 6\%$. We show that upon oxidation, LTG material can expand by $>25\%$ while crystalline material contracts by $<2\%$. Atomic force microscopy analysis indicates thickness-dependent variations in the oxide microstructure. Additionally, an optical scattering loss of $2.1 \times 10^{-4}\%$ /pass is calculated based on surface roughness measurements for a thin layer of oxidized crystalline material. © 1998 American Institute of Physics. [S0003-6951(98)03550-5]

Compound semiconductor native oxides formed by wet thermal oxidation of AlGaAs alloys¹ have been widely used in fabricating innovative and higher performance optoelectronic devices. This insulating and transparent oxide material has been used for current and optical-mode confinement in both edge-emitting² and vertical-cavity surface-emitting lasers.³ Native oxides have additionally been employed for the formation of broad-bandwidth distributed Bragg reflectors (DBRs).⁴ While the kinetics^{5,6} and microstructure⁷ of the oxidation reaction and resulting oxide have been studied, reports of the oxide's optical constants are lacking. The few refractive index values reported in the literature have been measured either by single-wavelength ellipsometry at 633 nm (see Refs. 8 and 9) or by extrapolating from the spectral shift in the peak reflectance of an oxidized $(\text{Al}_{0.98}\text{Ga}_{0.02})_x\text{O}_y$ -GaAs DBR.⁴

In this letter we report the optical constants of oxidized crystalline and low-temperature-grown (LTG) $\text{Al}_{0.98}\text{Ga}_{0.02}\text{As}$ films over the wavelength range of 240–1700 nm, as determined by variable angle spectroscopic ellipsometry.¹⁰ We additionally report the expansion/contraction coefficients and atomic force microscopy (AFM) analysis of the surface morphology of these oxide films. Lastly, we calculate optical scattering loss based on AFM measurements of surface roughness.

The samples consisted of a single $\text{Al}_{0.98}\text{Ga}_{0.02}\text{As}$ layer nominally 100–300 nm thick grown by molecular beam epitaxy as a digital alloy with a 6 nm (5.5 nm AlAs, 0.5 nm $\text{Al}_{0.50}\text{Ga}_{0.50}\text{As}$) period. The samples were grown at temperatures of 580, 350, and 250 °C, respectively, yielding crystalline, polycrystalline, and amorphous layers, as determined by reflection high-energy electron diffraction measurements. The polycrystalline and amorphous layers incorporate excess arsenic, resulting in nonstoichiometric layers. All samples were oxidized at 450 °C in a three-zone tube furnace under a 1 ℓ/min flow of nitrogen gas bubbled through deionized water at 75 °C. To limit atmospheric hydrolyzation, all samples were oxidized immediately upon removal from the reactor. The oxidation rate for the crystalline sample was determined

by reflectance fits to be ~ 35 nm/min. The oxidation rates for both LTG samples were significantly greater and will require *in situ* monitoring for a quantitative characterization of these thin surface layers.

Ellipsometry measures the polarization state (ψ and Δ) of a reflected monochromatic, polarized, collimated beam of light incident at a given angle to the sample normal.¹¹ In contrast to single-wavelength ellipsometry, variable angle spectroscopic ellipsometry measures the polarization state at multiple wavelengths and angles of incidence and thus minimizes the possibility of correlated variables in the regression analysis fit. This technique thereby allows the unique determination of optical constants, film thickness, and additional microstructural properties. The optical model used in our experiments was an oxide layer clad on top by a surface roughness layer and on the bottom by a thin interfacial layer. The fitting parameters of the model were the surface roughness thickness, the thickness of the oxide layer, the thickness of an interface layer between the substrate and oxide, three Cauchy coefficients describing the refractive index, and one parameter fitting a small thickness nonuniformity across the illumination spot of the ellipsometer. The optical constants of crystalline GaAs were collected from published literature.^{12–16} A Herzinger–Johs parametrized dispersion model¹⁷ was fit to the reference data to extract one set of optical constants for GaAs over the entire measured spectral range. These substrate optical constants were not permitted to vary during the fit. The refractive index of the oxide layer was modeled over the entire measured spectra range using a Cauchy dispersion function of the form $n(\lambda) = A + B/\lambda^2 + C/\lambda^4$. The thin interface or “intermix” layer between the oxide and the substrate was modeled as 50% GaAs and 50% oxide using a Bruggeman effective medium approximation.¹⁸ Similarly, the surface roughness layer was modeled as a 50/50 mixture of oxide and void. Data were acquired at three angles of incidence (65°, 70°, and 75°) over the range of 240–1700 nm in steps of 10 nm. All angles and wavelengths were fit simultaneously to maximize sensitivity to the model fitting parameters. Model fitting parameters and other quan-

TABLE I. Summary of parameters and quantities for the three samples.

Crystallinity	Crystalline	Polycrystalline	Amorphous
$T_{\text{Growth}} (^{\circ}\text{C})$	580	350	250
$t_{\text{Inlemix}} (\text{nm})$	1.9	24	4.5
$t_{\text{Oxide}} (\text{nm})$	164	418	228
$t_{\text{SR}} (\text{nm})$	0	33	7
A	1.5713	1.4297	1.4485
B	4.83×10^{-3}	1.14×10^{-2}	4.41×10^{-3}
C	9.67×10^{-5}	0	5.15×10^{-5}
$\% \text{Exp}$	$> -2\%$	$\sim 13\%$	$> 25\%$
α_{Scatter}	$2.1 \times 10^{-4}\%$	$> 1.6\%$	$6.6 \times 10^{-4}\%$

ties discussed are tabulated in Table I to serve as a reference throughout this letter.

For the oxidized crystalline (580 °C) sample, excellent fits to the measured ψ and Δ polarization functions were obtained without the addition of a surface roughness layer and with the inclusion of a thin 1.9 nm interfacial layer. A thin interface layer illustrates the atomic abruptness of the $(\text{Al}_{0.98}\text{Ga}_{0.02})_x\text{O}_y$ -GaAs interface and is consistent with reported high-resolution transmission electron-microscopy measurements.¹⁹ The complex refractive index determined for our 164-nm-thick sample indicates no measurable absorption over the entire spectra range from 240–1700 nm. The upper bound on the absorption is given by the noise in the measurement, and thus the extinction coefficient k is < 0.0015 at 240 nm. The Cauchy fitting coefficients for the real part of the refractive index are: $A = 1.5713$, $B = 4.83 \times 10^{-3}$, and $C = 9.67 \times 10^{-5}$, using λ in micrometers. The uncertainties in the $n(\lambda)$ functions reported in this letter are sample dependent and are in the third decimal place, based on measured uncertainties in the ψ and Δ measurement.

We have observed variations in the refractive index of up to 0.015 across several similarly grown and oxidized samples of different thicknesses. Figure 1 shows the index for three different sample thicknesses and error bars representative of third decimal place uncertainties. We observe a variation in the real index of $\pm 0.5\%$ for layer thickness variations of $\pm 6\%$. For these three sample, we observe a decreasing refractive index with increasing film thickness. The shape of the dispersion curves are similar, indicating

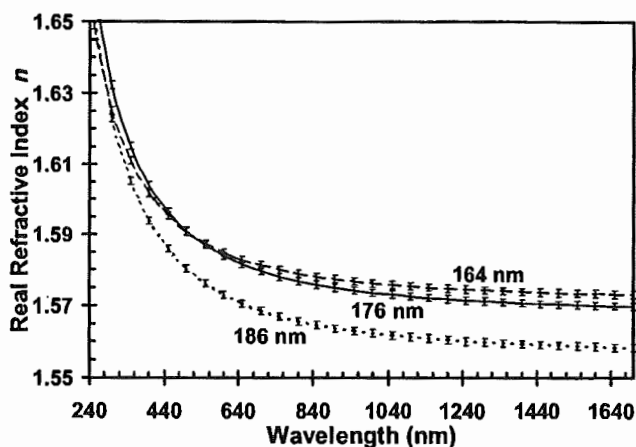


FIG. 1. Dispersion curves measured for three different sample thicknesses of oxidized crystalline material. Error bars representative of third decimal place uncertainties are shown.

that all three films are of the same material but different densities.

To obtain a measurement of the expansion or contraction of the oxide films, the reflectance of one quarter of the “as-grown” sample was measured using a spectrophotometer while another quarter was simultaneously oxidized. The as-grown sample’s reflectance spectrum was fit using Terry’s nine harmonic oscillator model²⁰ for the optical constants of $\text{Al}_{0.98}\text{Ga}_{0.02}\text{As}$ and GaAs, with the addition of a thin dry-oxidized cap layer whose index was approximated using the measured ellipsometric index data obtained for wet thermal oxidation. Comparison of the determined as-grown thickness to the oxide thickness measured by ellipsometry showed a $< 2\%$ contraction of the film.

For the oxidized LTG amorphous (250 °C) sample, fits to the measured ψ and Δ polarization functions were obtained with a 7 nm surface roughness layer and a 4.5 nm interfacial layer. The Cauchy fitting coefficients for the refractive index are: $A = 1.4485$, $B = 4.41 \times 10^{-3}$, and $C = 5.15 \times 10^{-5}$, using λ in micrometers. The absorption of this 228-nm-thick layer is again below instrumental sensitivity. The shape of the dispersion curves for the crystalline and amorphous samples are similar; however, the index of the amorphous sample is offset due to a lower A coefficient. This characteristic is again indicative of a lower density film of the same material. Comparing the as-grown thickness to the thickness of the oxide layer reveals a $> 25\%$ expansion of the oxide layer. One explanation for this large expansion is the large quantity ($\sim 10\%$) of excess arsenic incorporated into the layer at low growth temperatures.^{21,22} When the arsenic-rich layer is oxidized, the arsenic escapes,⁸ leaving voids that decrease the density of the oxide and lower the value of the A coefficient in the Cauchy fit. The reduced density is consistent with the observed increased oxidation rate as gas transport of reactants through the layer to the oxidation front is facilitated.⁷

For the oxidized LTG polycrystalline (350 °C), sample, fits to the measured ψ and Δ polarization functions were obtained with a 33 nm surface roughness layer and a 24 nm interfacial layer over the wavelength range of 900–1700 nm. The limited spectral range of a good fit suggests that the oxidation had not entirely consumed the LTG- $\text{Al}_{0.98}\text{Ga}_{0.02}\text{As}$ and a thin unoxidized, arsenic-rich layer remains below the oxide. The Cauchy fitting coefficients for the refractive index over the 900–1700 nm spectral range are: $A = 1.4297$, $B = 1.14 \times 10^{-2}$, and $C = 0$, using λ in micrometers. The extinction coefficient for this 419 nm sample is again below the noise limit of the measurement. An oxide layer expansion of $\sim 13\%$ was measured. Figure 2 displays the dispersion curves for the three samples grown at different temperatures. The large variation (> 0.1) in the refractive index with sample crystallinity is illustrated.

The surface morphology of the oxide films was studied by AFM, and representative images are shown in Fig. 3. Figure 3(a) is an image of the 164-nm-thick oxidized crystalline layer. The image shows elongated 1–1.5 μm features aligned with the $[01\bar{1}]$ direction atop a flat and uniform underlayer. Figure 3(b) shows an image of a ~ 400 -nm-thick oxidized crystalline layer. The elongated features are no longer visible, and cracking of the film is evident. The varia-

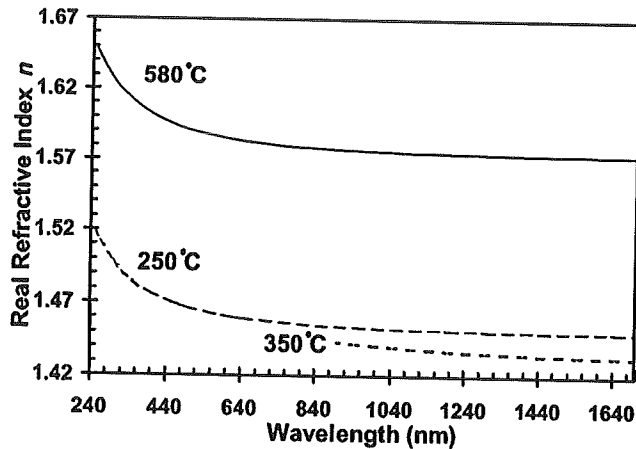


FIG. 2. Dispersion curve measured for the oxidized crystalline (580 °C), LTG polycrystalline (350 °C), and LTG amorphous (250 °C) samples. The large variation (>0.1) in the refractive index with sample crystallinity is illustrated.

tion in the surface morphology suggests variations in the complex microstructure of the oxide and its dependence on thickness, as also suggested by our refractive index measurements. The 228-nm-thick oxidized LTG, amorphous (250 °C) sample is shown in Fig. 3(c). Elongated features are again observable, but are oriented along the [011] direction and atop a grainy underlayer. Alignment of these features to a crystal axis in the amorphous sample suggests that the orientation is imposed by the crystalline substrate. Severe cracking is observed for the oxidized, 418 nm thick, LTG polycrystalline (350 °C) sample shown in Fig. 3(d). The cracks range in width from 50 to 300 nm and are several micrometers long. The severity of the cracking in the LTG sample as compared to an oxidized crystalline film of similar thickness [Fig. 3(b)] indicates regions of higher stress resulting from the larger volume change of the oxidized polycrystalline material.

Optical scattering loss for the first surface can be calcu-

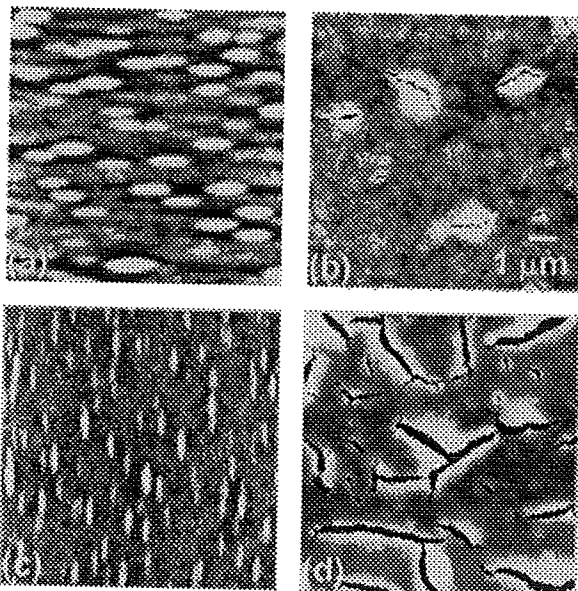


FIG. 3. AFM images of the oxide surface morphology for: (a) 164 nm thick, crystalline (580 °C), 10 nm z range, (b) ~400 nm thick, crystalline (580 °C), 100 nm z range, (c) 228 nm thick, LTG amorphous (250 °C), 25 nm z range, and (d) 418 nm thick, LTG polycrystalline (350 °C), 200 nm z range.

lated for the four samples of Fig. 3 using the root-mean-square (rms) roughness from the AFM data, assuming a Gaussian distribution of heights and normally incident illumination with a wavelength of 1 μm .²³ For the four samples in Figs. 3(a)–3(d), the calculated optical scattering loss per pass is $2.1 \times 10^{-4}\%$, $5.3 \times 10^{-2}\%$, $6.6 \times 10^{-4}\%$, and $>1.6\%$, respectively. The rms roughness of the 164 nm thick, oxidized crystalline layer is 0.5 nm, comparable to a plasma-enhanced chemical-vapor-deposited coating.

We have reported the optical constants of oxidized crystalline and LTG $\text{Al}_{0.98}\text{Ga}_{0.02}\text{As}$ over the wavelength range of 240–1700 nm. For oxidized crystalline material, we observe a variation in the real index of $\pm 0.5\%$ for layer thickness variations of $\pm 6\%$. We have shown that upon oxidation, LTG material expands, while crystalline material contracts. Furthermore, we calculate a low optical scattering loss for oxidized crystalline material based on analysis of AFM measurements. Knowledge of the dispersion characteristics of native-oxide films will aid device design and prove useful in the development of broad bandwidth, native-oxide antireflection coatings.

- ¹J. M. Dallesasse, N. Holonyak, Jr., A. R. Sugg, T. A. Richard, and N. El-Zein, *Appl. Phys. Lett.* **57**, 2844 (1990).
- ²J. M. Dallesasse and N. Holonyak, Jr., *Appl. Phys. Lett.* **58**, 394 (1991).
- ³D. L. Huffaker, D. G. Deppe, K. Kumar, and T. J. Rogers, *Appl. Phys. Lett.* **65**, 97 (1994).
- ⁴M. H. MacDougall, H. Zhao, P. D. Dapkus, M. Ziari, and W. H. Steier, *Electron. Lett.* **30**, 1147 (1994).
- ⁵M. Ochiai, G. E. Giudice, H. Temkin, J. W. Scott, and T. M. Cockerill, *Appl. Phys. Lett.* **68**, 1898 (1996).
- ⁶R. L. Naone, E. R. Hegblom, B. J. Thibeault, and L. A. Coldren, *Electron. Lett.* **33**, 300 (1997).
- ⁷R. D. Twesten, D. M. Follstaedt, K. D. Choquette, and R. P. Schneider, Jr., *Appl. Phys. Lett.* **69**, 19 (1996).
- ⁸A. R. Sugg, E. I. Chen, N. Holonyak, Jr., K. C. Hsieh, J. E. Baker, and N. Finnegan, *J. Appl. Phys.* **74**, 3880 (1993).
- ⁹E. F. Schubert, M. Passlack, M. Hong, J. Mannerts, R. L. Opila, L. N. Pfeiffer, K. W. West, C. G. Bethea, and G. J. Zydzik, *Appl. Phys. Lett.* **64**, 2976 (1994).
- ¹⁰All samples were characterized with the J. A. Woollam Company Variable Angle Spectroscopic Ellipsometer (VASE[®]) system. The data were acquired and analyzed using WVASE32 analysis software version 3.012. Trade name is to aid in duplicating the measurement and does not imply endorsement by the National Institute of Standards and Technology.
- ¹¹J. A. Woollam and P. G. Snyder, in *Encyclopedia of Materials Characterization* (Butterworth-Heinemann, Boston, 1992), p. 401.
- ¹²E. D. Palik, *Handbook of Optical Constants of Solids* (Academic, San Diego, 1985), p. 429.
- ¹³J. B. Theeten, D. E. Aspnes, and R. P. H. Chang, *J. Appl. Phys.* **49**, 6097 (1978).
- ¹⁴G. E. Jellison, Jr., *Opt. Mater.* **1**, 151 (1992).
- ¹⁵A. N. Pikhtin and A. D. Yas'kov, *Sov. Phys. Semicond.* **12**, 622 (1978).
- ¹⁶D. S. Gerber and G. N. Maracas, *IEEE J. Quantum Electron.* **29**, 2589 (1993).
- ¹⁷B. Johs, C. M. Herzinger, J. H. Dinan, A. Cornfeld, and J. D. Benson, *Thin Solid Films* **113–114**, 137 (1998).
- ¹⁸D. E. Aspnes, J. B. Theeten, and F. Hottier, *Phys. Rev. B* **20**, 3292 (1979).
- ¹⁹T. Takamori, K. Takemasa, and T. Kamijoh, *Appl. Phys. Lett.* **69**, 659 (1996).
- ²⁰F. L. Terry, Jr., *J. Appl. Phys.* **70**, 409 (1991).
- ²¹D. P. Docter, J. P. Ibbetson, Y. Gao, U. K. Mishra, T. Liu, and D. E. Grider, *J. Electron. Mater.* **27**, 479 (1998).
- ²²J. P. Ibbetson (private communication).
- ²³H. E. Bennett and J. O. Porteus, *J. Opt. Soc. Am.* **51**, 123 (1961).